CONF-840923--1

An analysis of measurements of the thermal conductivity of liquid urania

Joanne K. Fink, Leonard Leibowitz
Chemical Technology Division, Argonne National Laboratory, 9700 South Cass Avenue, Argonne, IL 60439, USA

Abstract. An analysis was performed of the three existing measurements of the thermal conductivity and thermal diffusivity of molten uranium dioxide. A transient heat transfer code [THTB] was used for this analysis. A much smaller range of values for thermal conductivity than originally reported was found: the orginal values ranged from 2.4 to 11 $W \cdot m^{-1} \cdot K^{-1}$, with a mean of 7.3 $W \cdot m^{-1} \cdot K^{-1}$, whereas the recalculated values ranged from 4.5 to 6.75 $W \cdot m^{-1} \cdot K^{-1}$, with a mean of 5.6 $W \cdot m^{-1} \cdot K^{-1}$.

CONF-840923--1

DE84 015806

1. Introduction

The thermal conductivity of reactor fuel is one of the more important thermophysical properties needed in reactor safety analysis. In certain areas, such as post-accident heat removal or molten fuel-coolant interactions, the thermal conductivity of fuel is particularly important. The first measurement of this quantity (Kim et al. 1977) employed a modulated electron beam method, which yielded the thermal diffusivity of molten urania. The value found was about five times greater than that of the solid at the melting point. This surprisingly high value was attributed to radiative heat transfer in the liquid. Subsequently, however, Bober et al. (Bober et al. 1981) showed this mechanism to be unlikely. Recently, two other measurements (Otter and Damien 1982, Tasman et al. 1983) of the thermal conductivity for liquid urania were reported. Otter and Damien (Otter and Damien 1982), using a laser-pulse method, found a value quite close to that of the earlier workers. In contrast, Tasman et al. (Tasman et al. 1983), using a novel quasi-stationary method, found that the thermal conductivity of urania fell slightly on melting. The two high results were questioned by Tasman et al. on the basis that, because tungsten containers had been used, there was the possibility of contamination of the sample with tungsten, as well as errors due to heat conduction through the containers walls. Because of the importance of thermal conductivity to reactor safety analysis, we undertook an extensive analysis of the three experiments to decide whether or not there were flaws in the heat transfer analysis of the results. Study of the importance of wall conduction in two of the experiments and detailed examination of the unique method of Tasman et al. was expected to lead to a better understanding of the reported results and aid in planning other experiments, if that seemed warranted.

We present here a summary of the results of the original workers followed by our analysis of the experiments. The chief tool for our analysis is the heat transfer code THTB (Transient Heat Transfer, Version B) developed by Kaganove (Kaganove 1982). This is a proprietary code, originally written by the General Electric Company, that analyzes three-dimensional heat transfer using a finite difference method. The basic function of the program is to set up the general heat balance equations for each node point, to compute the terms that apply from the input given, and to solve the resulting set of

NOTICE
PORTIONS OF THIS REPORT ARE ILLEGIBLE. It has been reproduced from the best available copy to permit the broadest possible availability.

MASTER

DISTRIBUTION OF THIS DOCUMENT IS UNLIMITED

DISCLAIMER

This report was prepared as an account of work sponsored by an agency of the United States Government. Neither the United States Government nor any agency thereof, nor any of their employees, makes any warranty, express or implied, or assumes any legal liability or responsibility for the accuracy, completeness, or usefulness of any information, apparatus, product, or process disclosed, or represents that its use would not infringe privately owned rights. Reference herein to any specific commercial product, process, or service by trade name, trademark, manufacturer, or otherwise does not necessarily constitute or imply its endorsement, recommendation, or favoring by the United States Government or any agency thereof. The views and opinions of authors expressed herein do not necessarily state or reflect those of the United States Government or any agency thereof.

equations for the central temperatures of the nodes by the Gauss-Seidel method. The program can treat the following heat-exchange modes: conduction, convection, gray-body diffuse radiation, surface flux, internal generation, non-sink mass flow, and latent heat effects.

2. Analysis of thermal conductivity measurements

2.1 Measurements of Kim et al.

Kim et al. used a modulated electron beam technique to measure the thermal diffusivity of UO_2. The theory for this method was developed by Cowan (Cowan 1961) and applied to solid urania by Wheeler (Wheeler 1965). In the measurements performed by Kim et al., a thin UO_2 sample clad in tungsten was heated with two electron beams. The top beam was modulated sinusoidally, and the difference in phase between the top and the bottom temperatures was measured. From the experimental phase changes, the thermal diffusivity of UO_2 was calculated. Measurements were reported on two thicknesses of UO_2--0.813 mm (0.032 in.) and 1.219 mm (0.048 in.)--and three modulation frequencies--0.25 Hz ($\pi/2$ rad$\cdot$s^{-1}), 0.50 Hz (π rad$\cdot$s^{-1}), and 0.75 Hz ($3\pi/2$ rad$\cdot$s^{-1}). Work was done at 0.75 Hz only for the thicker sample. The temperature varied somewhat from case to case. In analyzing these measurements, Kim et al. used a simple idealized three-layer model (Sparrow 1972) in which uniform heating and no side walls, i.e., an infinite disc, were assumed. Using THTB, we analyzed this ideal case (designated "the ideal model"), as well as the more realistic case of a container with tungsten side walls in which, as in the actual experiment, heating did not extend to the edge of the container (designated "the real model"). The time-temperature histories of the top and bottom faces for the UO_2 sample were followed using THTB. A separate computer code was written to determine the temperature maxima and minima of the top and bottom center of the sample and to calculate the phase shifts from the difference in time between successive maxima and minima. We studied five cases, corresponding to the five experimental combinations of modulation frequency and thickness. Phase shifts were found from the THTB models of heat transfer through the tungsten and UO_2 cells for the five cases using both the real and ideal models for thermal conductivities of liquid UO_2 ranging from 2 to 10 W$\cdot$m$^{-1}\cdot$K^{-1}. These calculated phase shifts were compared to the experimental values. Extensive tests were performed using the THTB models in order to ensure that the calculated phase shifts were insensitive to input parameters. Phase shifts as a function of thermal conductivity calculated using THTB for both the real and ideal models disagreed significantly with results reported by Kim et al. Therefore, the analysis employed by Kim et al. was reexamined.

Following the notation of Kim et al., the ideal model of the thermal diffusivity cell is shown in Fig. 1. Calculations were done for two cells: the thin cell with a UO_2 layer of 0.813 mm and the thick cell with a UO_2 layer of 1.219 mm. The width of the cell was assumed to be infinite.

Heat transfer in the three-layer cell is determined by the equation

$$\frac{\partial T_i}{\partial t} = \alpha_i \frac{\partial^2 T_i}{\partial x^2}, \quad i = 1,2,3 \tag{1}$$

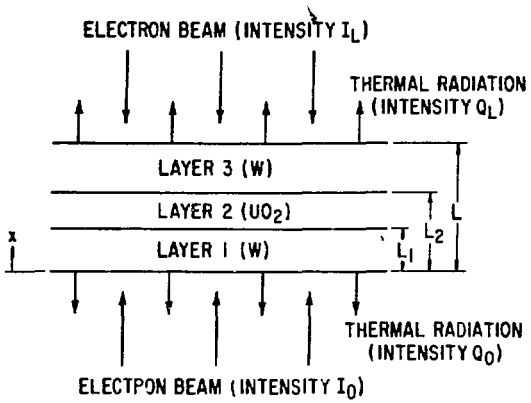

Figure 1. Ideal model for heat transfer study, $L_1 = 1.016$ mm, $L-L_2 = 1.40$ mm.

where T is the temperature, t is the time, α is the thermal diffusivity, and x is the distance from the bottom of the cell. The subscript i denotes the layers of the cell. The boundary conditions for Eq. 1 are

$$k_1 \frac{\partial T_1}{\partial x} = Q_0 - I_0 \qquad \text{at } x = 0 \tag{2}$$

$$\left.\begin{aligned} k_1 \frac{\partial T_1}{\partial x} &= k_2 \frac{\partial T_2}{\partial x} \\ T_1 &= T_2 \end{aligned}\right\} \quad \text{at } x = L_1 \qquad \begin{matrix}(3)\\(4)\end{matrix}$$

$$\left.\begin{aligned} k_2 \frac{\partial T_2}{\partial x} &= k_3 \frac{\partial T_3}{\partial x} \\ T_2 &= T_3 \end{aligned}\right\} \quad \text{at } x = L_2 \qquad \begin{matrix}(5)\\(6)\end{matrix}$$

$$k_3 \frac{\partial T_3}{\partial x} = -Q_L + I_L \qquad \text{at } x = L \tag{7}$$

where radiation to negligible temperature surroundings gives

$$Q_0 = \epsilon_1 \sigma T_1^4 \tag{8}$$

$$Q_L = \epsilon_3 \sigma T_3^4 \tag{9}$$

$$I_L = I_{LS} + A \sin \omega t \tag{10}$$

In the above equations, k is the thermal conductivity; ϵ is the emissivity; σ is the Stefan-Boltzmann constant (5.67×10^{-8} $J \cdot K^{-4} \cdot m^{-2} \cdot s^{-1}$); Q_0 and Q_L are the heat from radiation at x = 0 and L, respectively; and I_0 and I_L are the intensities of the electron beam at the bottom and top surfaces, respectively. The intensity of the electron beam at the bottom surface is constant, whereas that at the top surface is composed of a steady-state contribution, I_{LS}, and a time-dependent sine wave, sin ωt.

The time at which the cell reaches steady state is t = 0. At t = 0, the modulated heat flux from the sine-wave time-dependent electron beam is added to the top surface flux. The temperature at any point i, T'_i, is defined by

$$T'_i = T_i + \theta_i(x,t) \tag{11}$$

where T_i is the steady-state temperature. Substituting Eq. 11 into Eqs. 1-10 and keeping only highest order terms in T_i, results in 12 simultaneous equations for θ_i that agree with those repored by Kim et al. These equations, given in the Appendix, were solved numerically using matrix techniques (Dongarra et al. 1979).

The solution of these equations was checked by comparison with a single-layer case and the solution of Cowan (Cowan 1961); two three-layer cases (for frequency $\omega = \pi$ and $\omega = \pi/2$) were also checked by hand calculations. These three-layer calculations were considered essential because comparison with the single-layer case checks only 4 of the 12 simultaneous equations.

The phase shifts calculated for the ideal and real models with THTB are shown for two cases in Figs. 2-3. Also included in these figures is our reassessment of the Kim et al. measurements using the ideal analytical model. As can be readily seen, the curves of Kim et al. give significantly higher thermal conductivities for a given phase shift, whereas the three other curves are in reasonable agreement. From our calculation of the phase shift using the ideal model of Sparrow, we believe the errors in the analysis presented by Kim et al. occurred in the final formulation and programming of the matrix for the calculation of the solution to the twelve simultaneous equations.

The criticism of Tasman et al. that these experiments are unreliable because of wall conduction can be more readily understood in the light of the THTB results. The phase shifts as a function of thermal conductivity for the ideal and real models begin to diverge significantly below about 5-6 $W \cdot m^{-1} \cdot K^{-1}$. Thus, assuming a high value for the thermal conductivity for liquid UO_2 would lead one to conclude that wall conduction is not important, whereas assuming a low value would lead one to the opposite conclusion. Statistical tests by us showed no significant dependence of phase shift on temperature or cell within a given frequency and thickness. Although it was expected that the thermal conductivity (and, hence, the phase shift) would vary with temperature, the experimental data for the temperature range of 3180 to 3310 K are insufficient to confirm this expectation.

We have taken the THTB real model as the best representation of these experiments. The thermal conductivities found from the THTB real model are given for each case in Table 1.

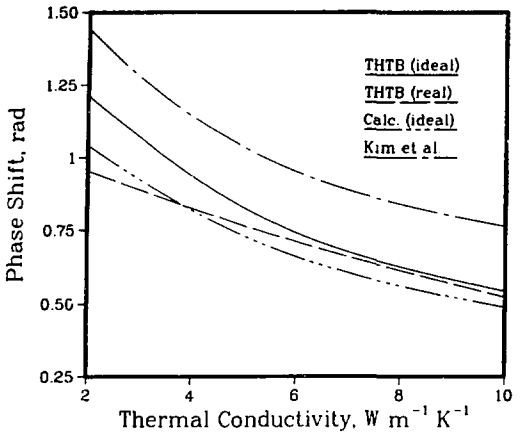

Figure 2. Calculated phase shifts as a function of molten UO_2 thermal conductivity: modulation frequency = 0.25 Hz, UO_2 thickness = 0.813 mm.

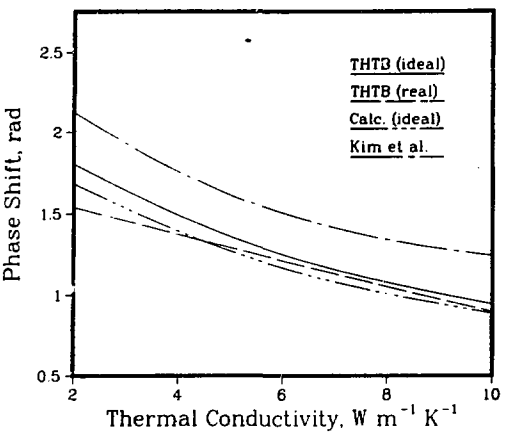

Figure 3. Calculated phase shifts as a function of molten UO_2 thermal conductivity: modulation frequency = 0.5 Hz, UO_2 thickness = 0.813 mm.

Table 1. Calculated thermal conductivity for THTB real model.

Sample Thickness, mm	Thermal Conductivity, $W \cdot m^{-1} \cdot K^{-1}$ frequency, $rad \cdot s^{-1}$		
	$\pi/2$	π	$3\pi/2$
0.813	4.6	5.0	--
1.219	6.8	5.9	6.0

Thermal conductivity values calculated using THTB ranged from 4.6 to 6.8 $W \cdot m^{-1} \cdot K^{-1}$ with a mean of 5.5 ± 0.91 $W \cdot m^{-1} \cdot K^{-1}$, whereas Kim et al. reported a mean value of 11 $W \cdot m^{-1} \cdot K^{-1}$. There is a statistically significant difference between the thermal conductivities found for the two different cell thicknesses. The means of the thermal conductivities are 6.4 ± 0.45 $W \cdot m^{-1} \cdot K^{-1}$ for the 1.219-mm thick cell and 4.8 ± 0.20 $W \cdot m^{-1} \cdot K^{-1}$ for the 0.813-mm thick cell. The meaning of this difference is not clear at present. It is possible that the tungsten and the molten UO_2 layer in the Kim et al. experiments were not in perfect contact, as was assumed in the THTB calculations. Contact resistance in the test cell would be relatively more important for the thin cell and would tend to give a lower calculated thermal conductivity. If this is correct, the higher thermal conductivity calculated from the thick cell should be weighted more heavily. Such speculation, however, seems unwarranted without additional data, and we believe that the experimental phase shifts reported by Kim et al. are best represented by a thermal conductivity of 5.5 $W \cdot m^{-1} \cdot K^{-1}$ with a standard deviation of 0.91.

2.2 Measurements of Tasman et al.

The thermal conductivity of liquid UO_2 was measured by Tasman et al. using a unique quasi-stationary method on a partially molten, self-contained sample. A horizontal disk of UO_2 (6 mm in diameter and 1.2-3 mm thick) was heated in an argon atmosphere using three continuous-wave CO_2 laser beams, two focused on the top and one focused on the bottom of the sample. Two of the beams focused $\leq$100 W onto a diameter of about 4 mm on the sample bottom and 2 mm on the sample top, and the third laser focused $\leq$20 W onto about 1-mm diameter of the sample top. The sample was heated only with the lower beam until a temperature of 1800°C was reached. The upper beams were then turned on, and a molten pool of UO_2 formed on the top of the sample. The peak temperature at the center of the top face was 3200°C. The melting experiment could only be carried out for about 4-5 seconds because of problems with vaporization of the sample. The authors report only minor sample loss during a 5 second exposure.

The thermal conductivity was determined from measurement of the depth of penetration of the melt front and comparison of it with calculated values of melt thickness as a function of thermal conductivity. The authors report a thermal conductivity for liquid UO_2 near the melting point of 2.2 ± 1 $W \cdot m^{-1} \cdot K^{-1}$, which is about 65% of the extrapolated value of the solid at the melting point.

This experiment was difficult to model with THTB because of the large number of nodes required to obtain the desired spatial resolution. Tests on the number of nodes were made to ensure that results were independent of the values selected. We found the fractional lower beam power needed to achieve a steady-state temperature of 1800°C at the bottom center of the UO_2 sample and allowed the calculation to proceed until steady state had been well established. At this point in the calculation, upper beam power was introduced and heating was continued until a new steady state had been reached. The THTB calculations were performed for liquid UO_2 thermal conductivities ranging from 2 to 10 $W \cdot m^{-1} \cdot K^{-1}$. The upper beam power was adjusted for each thermal conductivity so that the experimentally observed upper temperature of 3200°C was reached in five seconds. The fraction of maximum power needed ranged from 0.425 to 0.51 for the thermal conductivities studied.

We compare, in Fig. 4, the melt depth vs. thermal conductivity curve given by Tasman et al. (who assumed steady state) with the curves for the 5-second and steady-state melt depths calculated by THTB. We find a significant difference between these curves. The only experimental melt depth reported by Tasman et al. (about 0.22 mm) corresponds to a thermal conductivity of about 4.5 $W \cdot m^{-1} \cdot K^{-1}$ (using the 5-s THTB curve), which is higher than the 2.4 $W \cdot m^{-1} \cdot K^{-1}$ given by Tasman et al. for this single point.

The source of the difference between the Tasman et al. and the THTB steady-state curves is unclear. In any case, the thermal conductivity reported by Tasman et al. is too low, at least in part because of their assumption of steady state.

2.3 Measurements of Otter and Damien

The thermal diffusivity of molten UO_2 at the melting point was measured by Otter and Damien using a flash laser technique. This procedure, in widespread use for many years, has been very well studied. In this method, the sample is held in a furnace at constant temperature and one face is heated rapidly by

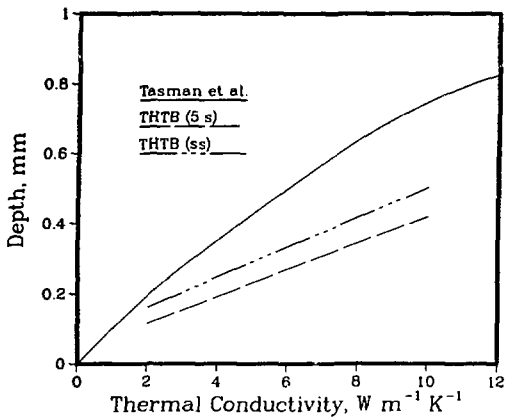

Figure 4. Calculated melt depth as a function of UO_2 thermal conductivity.

a laser. The time for the opposite face to rise to half its maximum temperature, $t_{1/2}$, is measured. In the Otter and Damien experiment, the UO_2 samples were sealed in flat tungsten cells, and the thermal diffusivity of the liquid UO_2 calculated from the half time of the tungsten and UO_2 composite. Results of these diffusivity measurements generally confirm the previous measurements by Kim et al. (Kim et al. 1977).

For this THTB calculation, the furnace environment was simulated by the boundary conditions of insulation at the top, bottom, and sides of the sample. The initial temperature was set at 3273 K. A surface flux on the top face simulated the laser pulse. The temperature rise of the bottom face as a function of time for 1.5 seconds was calculated for a range of UO_2 thermal conductivities. The resulting $t_{1/2}$ values were used in the subsequent analysis. Because the THTB calculation shows a peak temperature increase that is above the temperature increase of the center of the bottom face at 1.5 seconds (effectively t_∞), the half times calculated from these two temperature increases are not identical. The difference in half times as a function of thermal conductivity is shown in Fig. 5.

Otter and Damien do not give their experimental half times and provide no details of their analysis of the experimental data. To compare the THTB calculations with the Otter and Damien experimental results, we calculated half times from their reported thermal diffusivities. Otter and Damien refer to a paper by Otter and Vandevelde (Otter and Vandevelde 1982) that gives two methods of analysis for a three-layer composite sample: (1) a three-layer extension of the mathematical "two-layer model of Larson and Koyama" (Larson and Koyama 1968) and (2) a Crank-Nicolson (Crank and Nicolson 1947) numerical finite difference model that takes into account losses to the external environment at high temperature. The three-layer model of Otter and Vandevelde does not account for thermal losses. We used the three-layer model given by Otter and Vandevelde to determine half times from the thermal diffusivities reported by Otter and Damien. In Fig. 5, these half times are plotted, along with the half times relative either to peak (THTB peak) or 1.5 second (THTB 1.5 s) temperatures calculated using the heat transfer code THTB. Table 2

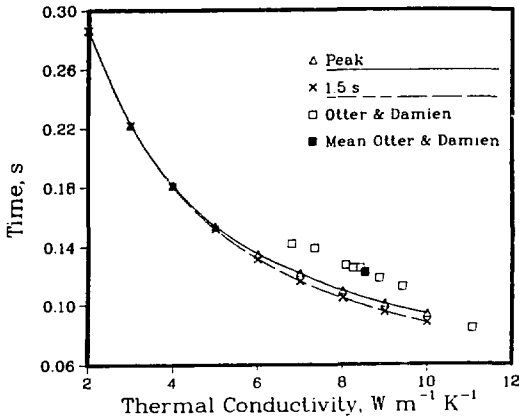

Figure 5. Calculated half times as a function of thermal conductivity for THTB model and Otter and Vandevelde three-layer model applied to the Otter and Damien experiment.

Table 2. Thermal conductivity for Otter & Damien half times.

	Half time, s	Thermal Conductivity, $W \cdot m^{-1} \cdot K^{-1}$		
		Otter & Damien	THTB Peak	THTB 1.5 s
max.	0.083	11.06	12.0	10.8
min.	0.149	6.8	5.2	5.1
mean	0.122	8.53	6.9	6.6

gives the maximum, minimum, and mean thermal conductivities reported by Otter and Damien, as well as those calculated using THTB with the half times determined from the three-layer model of Otter and Vandevelde.

The THTB calculations give 6.75 $W \cdot m^{-1} \cdot K^{-1}$ for the Otter and Damien mean half time (0.122 s), which is significantly lower than the mean of the thermal conductivities reported by Otter and Damien, 8.53 $W \cdot m^{-1} \cdot K^{-1}$. Differences in these calculations may arise from Otter and Damien's incorporation of heat losses with the Crank-Nicolson finite difference method; these heat losses are not included in the THTB calculation. Because the actual experimental half times are not published, it is impossible to determine conclusively the source of the discrepancy.

To test the reliability of the THTB calculations for the laser-pulse experiment and to assess the importance of heat losses in this experiment, the THTB code was applied to the experimental laser-pulse results of Blomquist on sapphire at 1207 K (Blomquist 1983). Calculations were done with and without taking into account radiation heat losses from sides, top and bottom of the sample. Half times with and without radiation heat losses differed by less than 1%. The results of the THTB calculations agree with the measured half time and corresponding thermal conductivity; these lie within the range of values for the thermal conductivity reported by the Thermophysical Properties Research Center (TPRC) (Touloukian et al 1970) at Purdue University. Although our calculation showed that radiation losses are unimportant for this laser-pulse experiment, the Otter and Damien experiment was at a significantly higher temperature, where radiation losses could become important, provided the sample temperature is increased significantly above the furnace temperature.

3 Discussion and conclusions

3.1 Recommendations and conclusions

Table 3 summarizes the reported experimental values for the thermal conductivity of liquid UO_2 at its melting point and the values calculated from our THTB models of these experiments. Our recommendation for the thermal conductivity of liquid UO_2 at its melting point is the mean of the THTB calculations from the three experiments, 5.6 ± 1.1 $W \cdot m^{-1} \cdot K^{-1}$.

Table 3. Reported and Calculated Thermal Conductivity of Liquid UO_2

Experiment	Reported Value, $W \cdot m^{-1} \cdot K^{-1}$	THTB Value, $W \cdot m^{-1} \cdot K^{-1}$
Kim et al. [1]	11	5.5
Tasman et al. [3]	2.4	4.5
Otter & Damien [2]	8.5	6.75

The THTB calculations for these three experiments have helped to clarify the sources of previous disagreements. The high value for the thermal conductivity reported by Kim et al. was due to errors in their solution of their simultaneous equations. The low value reported by Tasman et al. resulted, in part, from the assumption of steady-state conditions that were not actually present.

The range in the THTB values given in Table 3 is not surprising because of uncertainties in the experiments that have yet to be resolved. The solubility of tungsten in the UO_2 is an uncertainty that affects the results of both the experiment by Kim et al. and the Otter and Damien experiment. In addition, the absence of the experimentally determined half times for the

Otter and Damien experiment creates a large uncertainty in the THTB calculations of this experiment. Tasman et al. state that the largest uncertainty in their experimental procedure is the determination of the temperature profile of the top and bottom faces. Because these profiles are critical input to the modeling of this experiment, this creates a significant uncertainty in the calculated results. Another uncertainty in this experiment is the depth of the molten zone, because measurement of the melt depth of fuel after solidification may not be a reliable means of determination of the depth of molten material. Ackermann (Ackermann 1955) reported the melting point of UO_2 to be between 2661 and 2699 K, based on the appearance of residues from two series of experiments for which these were the maximum temperatures. Since the melting point was identified as 3120 K (Rand et al 1978) from thermal arrest data (Latta and Fryxell 1970, Lyon and Bailey 1967, Bates 1970) and enthalpy data (Hein and Flagella 1980, Leibowitz et al 1971) and a solid-solid phase transition was identified at 2670 K (Rand et al. 1978, Fink 1982, Leibowitz, Fink, and Slagle 1983), it seems likely that the difference in appearance observed by Ackermann was due to the solid-solid phase transition rather than melting. Thus, it is unclear whether visual observation of the cooled sample is a reliable method to distinguish UO_2 that is molten from UO_2 that is above the solid-solid phase transition but below the melting point.

Acknowledgments. We are very grateful to J. Kaganove for his assistance with the use of the computer code THTB. W. A. Ragland's helpful comments on the availability of graphic interfaces to THTB and D. R. Pedersen's suggestions on the use of THTB are also gratefully acknowledged.

References

Ackermann R. J., 1955 report ANL-5482, Argonne National Laboratory, Argonne, IL, USA

Bates J. L., 1970 J. Nucl. Mater 36, 234-236

Blomquist R. A., 1983 private communication to J. K. Fink ANL

Bober M., Singer J., Wagner K., 1981 Determination of the Optical Constants of Liquid UO_2 from Reflectivity Measurements, Proc. Eighth Symp. on Thermophysical Properties, J. V. Singers, Ed., American Society of Mechanical Engineers, New York, Vol. II, pp. 234-244

Cowan R. D., 1961 J. Appl. Phys. 32, 1363-1370

Crank J., Nicolson P., 1947 Proc. Camb. Phil. Soc. 43, 50-67

Dongarra J. J., Moler C. B., Bunch J. R., Stewart G. W., 1979 report Linpack User's Guide, Society for Industrial and Applied Mathematics (SIAM), Philadelphia

Fink J. K., 1982 Int. J. Thermophys. 3, 165-200

Hein R. A., Flagella P. N., 1968 General Electric Report GEMP-578, Nuclear Technology Division General Electric Co., USA

Kaganove J., 1982 report TM281 Revised, Argonne National Laboratory, Argonne, IL, USA

Kim C. S., Haley R. A., Fischer J., Chasanov M. G., Leibowitz L., 1977 Measurement of Thermal Diffusivity of Molten UO_2, Proc. Seventh Symp. on Thermophysical Properties, A. Cezairliyan, Ed., American Society of Mechanical Engineers, New York, p. 338-343

Larson K. B., Koyama K., 1968 J. Applied Phys. 34, 4408-4416

Latta R. E., Fryxell R. E., 1970 J. Nucl. Mater. 35, 195-210

Leibowitz L., Chasanov M. G., Mishler L. W., Fischer D. F., 1971 J. Nucl. Mater. 39, 115-116

Leibowitz L., Fink J. K., Slagle O. D., 1983 J. Nucl. Mater. 116, 324-325

Lyon W. L., Bailey W. E., 1967 J. Nucl. Mater. 22, 332-339

Otter C., Damien D., 1982, Mesure de la Diffusivite Thermique de UO_2 Fondu, presented at the Eighth European Thermophysical Properties Conf., Baden-Baden, F. R. Germany, September 28-October 1, 1982

Otter C., Vandevelde J., 1982 Rev. Int. Hautes Temp. Refract. 19, 41-53

Rand M. H., Ackermann R. J., Gronvold F., Oetting F. L., Pattoret A., 1978 Rev. Int. Haute Temp. Refract. 15, 355-365

Sparrow E. M., 1972 private communication to M. G. Chasanov, ANL

Tasman H. A., Pel D., Richter J., Schmidt H. E., 1983, High Temp-High Pressures 15, 419-431

Touloukian Y. S., Powel R. W., Ho C. Y., Klemens P. G., 1970 Thermophysical Properties of Matter, Vol. 2: Thermal Conductivity Nonmetallic Solids, Plenum Press, New York, pp. 93-119

Wheeler M. J., 1965 Brit. J. Appl. Phys. 16, 365-376

Appendix

The change in temperature due to the sine wave modulation, denoted by $\theta_i(x,t)$ is represented by Eq. A-1 with the boundary conditions A-2 through A-6.

$$\frac{\partial\theta_i}{\partial t} = \alpha_i \frac{\partial^2\theta_i}{\partial x^2}, \qquad i = 1,2,3 \tag{A-1}$$

$$k_1 \frac{\partial\theta_1}{\partial x} = 4\varepsilon_1\sigma\theta_1 T_1^3 \qquad \text{at } x = 0 \tag{A-2}$$

$$\left.\begin{aligned} k_1 \frac{\partial\theta_1}{\partial x} &= k_2 \frac{\partial\theta_2}{\partial x} && \text{(A-3)} \\ \theta_1 &= \theta_2 && \text{(A-4)} \end{aligned}\right\} \text{at } x = L_1$$

$$\left.\begin{aligned} k_2 \frac{\partial\theta_2}{\partial x} &= k_3 \frac{\partial\theta_3}{\partial x} && \text{(A-5)} \\ \theta_2 &= \theta_3 && \text{(A-6)} \end{aligned}\right\} \text{at } x = L_2$$

$$k_3 \frac{\partial\theta_3}{\partial x} = -4\varepsilon_3\sigma T_3^3\theta_3 + A \sin \omega t \qquad \text{at } x = L$$

The solutions for θ_i are represented as

$$\theta_i(x,t) = f_i(x)\sin(\omega t) + g_i(x)\cos(\omega t), \quad i = 1,2,3 \tag{A-7}$$

where $f_i(x)$ and $g_i(x)$ are defined by

$$\frac{d^2 f_i}{dx^2} + \frac{\omega}{\alpha_i} g_i = 0, \qquad i = 1,2,3 \tag{A-8}$$

$$\frac{d^2 g_i}{dx^2} - \frac{\omega}{\alpha_i} f_i = 0, \qquad i = 1,2,3 \tag{A-9}$$

$$f_i(x) = e^{\lambda_i x}(A_i \sin\lambda_i x + B_i \cos\lambda_i x) + e^{-\lambda_i x}(C_i \sin\lambda_i x + D_i \cos\lambda_i x) \tag{A-10}$$

$$g_i(x) = e^{\lambda_i x}(B_i \sin\lambda_i x + A_i \cos\lambda_i x) + e^{-\lambda_i x}(-D_i \sin\lambda_i x + C_i \cos\lambda_i x) \tag{A-11}$$

$$\lambda_i = \sqrt{\frac{\omega}{2\alpha_i}} \tag{A-12}$$

In terms of f_i and g_i, the boundary conditions are

$$\left.\begin{aligned} k_1 \frac{df_1}{dx} - 4\epsilon_1 \sigma T_0^3 f_1 &= 0 \quad (A\text{-}13) \\ k_1 \frac{dg_1}{dx} - 4\epsilon_1 \sigma T_0^3 g_1 &= 0 \quad (A\text{-}14) \end{aligned}\right\} \text{ at } x = 0$$

$$\left.\begin{aligned} k_1 \frac{df_1}{dx} - k_2 \frac{df_2}{dx} &= 0 \quad (A\text{-}15) \\ k_1 \frac{dg_1}{dx} - k_2 \frac{dg_2}{dx} &= 0 \quad (A\text{-}16) \\ f_1 - f_2 &= 0 \quad (A\text{-}17) \\ g_1 - g_2 &= 0 \quad (A\text{-}18) \end{aligned}\right\} \text{ at } x = L_1$$

$$\left.\begin{aligned} k_2 \frac{df_2}{dx} - k_3 \frac{df_3}{dx} &= 0 \quad (A\text{-}19) \\ k_2 \frac{dg_2}{dx} - k_3 \frac{dg_3}{dx} &= 0 \quad (A\text{-}20) \\ f_2 - f_3 &= 0 \quad (A\text{-}21) \\ g_2 - g_3 &= 0 \quad (A\text{-}22) \end{aligned}\right\} \text{ at } x = L_2$$

$$\left.\begin{aligned} k_3 \frac{df_3}{dx} - 4\epsilon_3 \sigma T_L^3 f_3 &= A \quad (A\text{-}23) \\ k_3 \frac{dg_3}{dx} - 4\epsilon_3 \sigma T_L^3 g_3 &= 0 \quad (A\text{-}24) \end{aligned}\right\} \text{ at } x = L$$